



Heat transfer of water-based carbon nanotube nanofluids in the shell and tube cooling heat exchangers of the gasoline product of the residue fluid catalytic cracking unit

S. Masoud Hosseini¹ · Mohammad Reza Safaei^{2,3} · Patrice Estellé⁴ · S. Hadi Jafarnia¹

Received: 5 April 2019 / Accepted: 6 September 2019 / Published online: 21 September 2019
© Akadémiai Kiadó, Budapest, Hungary 2019

Abstract

In this study, a series of low-concentration carbon nanotubes (CNT) water-based nanofluids (0.0055, 0.055, 0.111 and 0.278 vol%) were used as coolants in a shell and tube cooler of the residue fluid catalytic cracking gasoline product to analyze their effects on heat performance of the heat exchanger. The coolants and gasoline flow in tube side and shell side, respectively. This work was performed through simulating the heat exchanger by ASPEN HTFS+ 7.3 software. The performance of the nanofluids to heat transfer was analyzed in comparison with cooling water. Results illustrated that 0.055% CNT concentration could enhance heat transfer properties of the heat exchanger such as Nusselt number, total heat transfer coefficient and heat transfer rate more than other concentrations. Therefore, the lowest temperature of outlet shell-side fluid was also observed at this concentration. Moreover, increment in mass flow rates of both the tube-side and shell-side fluids caused enhancement of the heat transfer, especially with 0.055 vol% CNT. Although there is an optimum concentration among the studied CNT volume fractions, all nanofluids exhibit better thermal performance of the heat exchanger than cooling water, whereas pressure drop increases with CNT loading.

Keywords Tube and shell heat exchanger · Carbon nanotube water-based nanofluids · Concentration · Mass flow rate · Thermal performance

List of symbols

A_t	Flow area of tube side (m ²)	h_{ss}	Convection heat transfer coefficient for shell-side fluid (W m ⁻² K ⁻¹)
A_s	Total heat transfer area of tube outside (m ²)	h_{nf}	Convection heat transfer coefficient for nanofluid (W m ⁻² K ⁻¹)
A_{cf}	Area of cross-flow (m ²)	h_{hot}	Convection heat transfer coefficient for hot fluid (W m ⁻² K ⁻¹)
C_{min}	Minimum specific heat (J kg ⁻¹ K ⁻¹)	k_{nf}	Thermal conduction for nanofluid (W m ⁻¹ K ⁻¹)
C_p	Fluid specific heat (J kg ⁻¹ K ⁻¹)	k	Thermal conduction for shell-side fluid (W m ⁻¹ K ⁻¹)
C_μ	Viscosity improvement coefficient	k_w	Thermal conduction for tube (W m ⁻¹ K ⁻¹)
d_i	Inner tube diameter (m)	m_{nf}	Nanofluid mass flow rate (kg s ⁻¹)
d_o	Outside tube diameter (m)	m_{ss}	Shell-side fluid mass flow rate (kg s ⁻¹)
D_e	Equivalent diameter (m)	Nu_{nf}	Nusselt number of nanofluid
		Pr_{nf}	Prandtl number of nanofluid
		Pr_{ss}	Prandtl number of shell side
		f	Friction factor
		q	Heat transfer rate (kW)
		T_{hi}	Hot fluid outlet temperature (°C)
		T_{ci}	Cold fluid outlet temperature (°C)
		Re_{ss}	Shell-side fluid Reynolds number
		Re_{nf}	Nanofluid Reynolds number

✉ Patrice Estellé
Patrice.estelle@univ-rennes1.fr

¹ Chemical and Process Engineering Department of the RFCC Unit, Arak Oil Refining Company, Arak, Iran

² Division of Computational Physics, Institute for Computational Science, Ton Duc Thang University, Ho Chi Minh City, Vietnam

³ Faculty of Electrical and Electronics Engineering, Ton Duc Thang University, Ho Chi Minh City, Vietnam

⁴ Univ Rennes, LGCGM, EA3913, F-35000 Rennes, France

U	Total heat transfer coefficient ($\text{W m}^{-2} \text{K}^{-1}$)
μ_{nf}	Nanofluid viscosity (mPa s)
μ_{bf}	Base fluid viscosity (mPa s)
μ_{ss}	Shell-side fluid viscosity (mPa s)
ϕ	Nanoparticle volume fraction
ΔT_{LMTD}	Log mean temperature difference ($^{\circ}\text{C}$)
ε	Effectiveness of heat exchanger

Introduction

Nanofluids are engineered colloidal suspensions of nanoparticles < 100 nm in a base fluid, which have recently been proposed as new generation of heat transfer fluids. Various nanoparticles have been selected to produce nanofluids, including metals [1, 2], metal oxides [3, 4] and nonmetals [5, 6]. These suspensions exhibit noticeably higher thermal conductivity than the pure liquid [7] which could improve heat transfer in heat exchangers [8, 9] since low thermal conductivity of the process fluids like water, ethylene glycol and industrial oils [1, 2, 10, 11] prevents high effectiveness of heat exchangers through making their heat transfer capability limited. Therefore, in most applications in which cooling or heating processes are performed by conventional fluids, nanofluids could be used rather than common single-phase fluids. For instance, nanofluids can be used in refrigerators, solar heaters, heating and cooling of buildings, radiators of cars, condensing and evaporating systems, oil recovery, medicine drug delivery and any type of liquid-based heat exchangers [12–20].

Heat exchangers are important devices in chemical processes and industries in the field of energy and heat transfer. One of the heat exchanger types is shell and tube one which is used in oil and gas industries, for example.

In recent years, the use of nanofluids in the heat exchangers, like shell and tube type, has thoroughly been recognized as a promising possibility in order to enhance heat transfer performance and save energy in various processes [21].

Barzegarian et al. [22] used Al_2O_3 –water nanofluids in a shell and tube heat exchanger and evaluated the effect of friction factor, Reynolds number and nanoparticles volume fraction on the heat performance. This work was performed under laminar flow condition. They found that the total heat transfer coefficient and thermal performance factor could be improved by increasing Re and nanoparticles volume fraction. For example, with 0.3vol% in Al_2O_3 nanoparticles, the total heat transfer coefficient and thermal

performance factors are increased by 29.8% and 18.9%, respectively, with a weak increase in the pressure drop.

Likewise, similar nanofluids were investigated by Shahrul et al. [23] in a tube and shell heat exchanger. They studied the effect of mass flow rate of both the shell and tube sides. The heat exchanger performance was analyzed, and the results were compared with water. These experiments demonstrated that the total heat transfer coefficient increased up to 26% in comparison with water and greatest performance was observed at 7 LPM flow rate.

Hosseini et al. [24] studied CNT–water nanofluid with low volume fractions. The performance of an industrial heat exchanger was simulated by heat exchanger design, rating and simulation software in laminar flow regime. They concluded that with increase in CNT concentration, heat transfer properties would be increased so that the total heat coefficient is 14.5% higher and heat rate reached 10.3% for the highest volume concentration. Furthermore, increasing CNT concentration caused reduction in temperature of the outlet of the shell-side fluid compared with water. It was demonstrated that increasing mass flow rate could increase heat transfer. Increase in pressure drop and pumping power was reported to be small and negligible.

Al-Abdali et al. [25] also conducted an experimental investigation on water-based Al_2O_3 nanofluid to determine the evolution of the friction factor and Nusselt number in a tube and shell heat exchanger. The tubes were finned and without fin. The Reynolds number was changed from 3000 to 10,500, and also the nanofluid volume concentration was 0.1%, 0.2% and 0.3%. It was observed that Nusselt number and friction factor increased with nanofluid concentration. Increasing Re (increasing turbulence) led to higher Nusselt number. At highest nanofluid concentration (0.3%), the Nusselt number increased by 25.6% for tube without fin. For finned tube, Nusselt number increased by 11.8% for highest Reynolds number ($Re = 10,500$) and highest nanofluid concentration of 0.3%.

Aghabozorg et al. [26] used nanofluid made of distilled water and Fe_2O_3 –CNT magnetic nanoparticle in a horizontally positioned tube and shell heat exchanger. They carried out test under various flow conditions (laminar, transient and turbulent flows) and three different heat fluxes. The results showed that increasing ϕ and T results in higher convection heat transfer coefficient. The heat transfer coefficient of the nanofluid was higher than base fluid. At $\phi = 0.1\%$, heat transfer increased by 13.54% and 27.69% for laminar and turbulent flows. For $\phi = 0.2\%$, the heat transfer coefficient increased by 34.02% and 37.50% in comparison with distilled water for laminar and turbulent flows conditions, respectively.

Many works performed on heat transfer of nanofluids in various types of heat exchangers are experimental. Although experimental studies are worthwhile approaches

to research, they go with some disadvantages such as determining difficultly contribution of physical phenomena to the system as well as the possible high expense of experiments that are obstacles for doing experimental studies because they require a large amount of sample or specific technical developments. Thus, modeling and simulations can be beneficial and good alternative to experiments because of lower cost, time saving and useful detail data and results on the studied system [27]. However, this requires using appropriate models for thermophysical properties or reliable experimental data.

In the current study, simulation of the residue fluid catalytic cracking unit (RFCC) gasoline product shell and tube cooler was carried out by using CNT–water nanofluids as coolant in low nanoparticle volume fractions. The simulation was performed considering real experimental data for nanofluids as done in previous works with different configurations such as square cavity [28], pipe [29] and microchannel heat sink [30]. The heat transfer performance of the RFCC was analyzed considering the influence of nanofluid concentrations and fluid mass flow rate.

Problem definition

One of the oil-refining units (in Arak Petroleum Refinery, Iran) is called RFCC (residue fluid catalytic cracking). There is a debutanizer tower in this unit where gasoline and LPG, produced through RFCC process, are separated from each other in this tower as LPG is up-flow and gasoline is bottom one. Outlet gasoline product from debutanizer column bottom, after passing through six air coolers, flows through the shell sides of two shell and tube heat exchangers in order to be more cooled by cooling water flows in tubes. Figure 1 illustrates these real shell and tube heat exchangers that are investigated in this study.

A branch of the cooled gasoline is utilized as the absorber fluid in a LPG absorption column (is called primary absorber). Therefore, the gasoline temperature is a very significant item since, generally, temperature is a vital factor in absorption process and this justifies the use of the mentioned heat exchangers for regulating (decreasing) the temperature of the gasoline.

During the warm seasons of the year, the air coolers could not be entirely capable of working on total duty. Likewise, temperature of the cooling water supplied by power plant and flowing in the tubes increases and exceeds 25 °C because of high ambient temperature. Therefore, cooling performance efficiency in the shell and tube heat exchanger decreases. Consequently, outlet temperature of shell-side gasoline rises, leading to lower absorption efficiency in the primary absorber column, causing loss of LPG through top flow. Enhancing the thermal properties of



Fig. 1 Real shell and tube cooling heat exchangers of the RFCC gasoline product that have been modeled. (1) Inlet cooling water to tubes, (2) outlet cooling water from tubes, (3) inlet gasoline product to shell, (4) outlet gasoline product from shell

the heat transfer fluids is one of the methods for solving this problem. With this goal, the use of water-based nanofluid containing carbon nanotubes in the heat exchanger has been analyzed numerically.

Modeling

The calculations for heat exchangers design and simulation are hugely difficult and complicated. For instance, to design a heat exchanger, many initial guesses must be considered which makes calculations really irritating and boring as well as increases probability of error in results. But, by using the software, all these calculations are performed by computer with noticeably faster pace just through applying the operational condition and the properties of working fluids as well as much more precise results would be available.

ASPEN HTFS+ 7.3 is useful software to simulate, design and evaluate the performance of the various types of heat exchangers such as shell and tube, plate, kettle and air cooler heat exchanger. This software is more comprehensive in data bank and the applications and features than the others like B-JAC software. HTFS+ has four calculation modes such as design, checking, simulation and maximum fouling.

Among the mentioned calculation modes, simulation mode is here considered to simulate the shell and tube heat exchanger described in Fig. 1. Within this mode, the heat exchanger specifications, the composition and operational/process condition of the shell-side and tube-side fluids and the cooling fluid thermophysical properties are entered into the software as inlet data. Then, after running the software,

it makes the outlet fluids process condition and heat transfer rate available. Water-based CNT nanofluids were introduced as cooling fluids. It is mentionable that thermophysical properties of the shell-side fluid (gasoline) are calculated by the software through the composition and process condition. For thermophysical properties of the nanofluid as tube-side cooling fluid, the data from Halefadl et al. [31] were used in order to supply input data for the simulation software. Volume fractions of the nanofluids were 0.0055%, 0.055%, 0.111% and 0.278%. More details about nanofluids characterization and properties evaluation can be found elsewhere [31]. Figure 2 expresses the influence of temperature and CNT loading effects on the thermophysical properties of presently used CNT nanofluids [31]. Because of turbulent flow involved within the tube of the heat exchanger, viscosity data of the CNT–water nanofluids used are reported in Fig. 2 for high shear rate. All other data necessary for the simulation process are gathered in Tables 1 and 2. Table 1 presents gasoline composition. Likewise, Table 2 contains

information about heat exchanger geometry. Figure 3a [32] and 3b (given from the software) also demonstrates schematically some geometry specifications as well as the flow parameters.

At first, the simulation was performed with water as cooling fluid to ensure validity of the results. After that, nanofluid simulations were carried out.

Results and discussion

Influence of the nanoparticle concentration on thermal performance of tube and shell sides at constant mass flow rates

Figure 4 shows the nanofluid Reynolds number Re_{nf} , evaluated from Eq. (1), as a function of CNT concentration at constant $\dot{m} = 81.74 \text{ kg s}^{-1}$ in tube side. It is observed that Re_{nf} decreases by increasing CNT concentration due to the increase of nanofluid viscosity with the content in

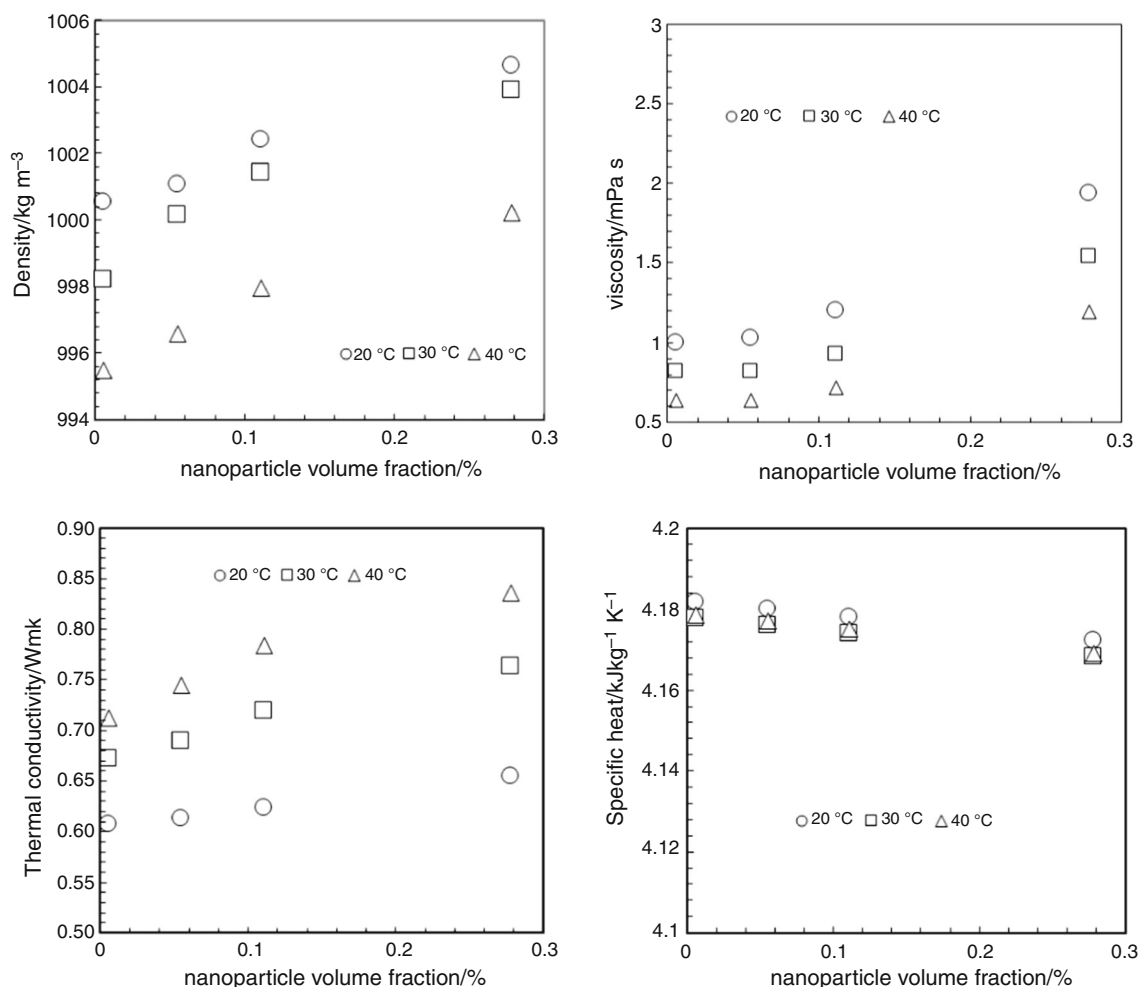


Fig. 2 Effects of temperature and CNT volume fraction on the thermophysical properties of nanofluids from [31]

Table 1 Composition of gasoline (shell-side fluid)

Component name	kmol/h	Component name	kmol/h
H ₂ O	1.7E-16	=N ₁ C ₄	2.87
CO	3.3E-18	=T ₂ C ₄	10.51
CO ₂	5.3E-19	=C ₂ C ₄	16.80
H ₂ S	1.E-10	IC ₄	2.64
=C ₂	2.5E-18	NC ₄	10.45
C ₂	1.E-14	=IC ₅	669.97
=C ₃	0.00022	IC ₅	357.84
C ₃	0.00067	NC ₅	63.50
=IC ₄	2.65	C ₆₊ (Product)	3458.56

nanotubes. Range values of Re_{nf} indicate that the flow is under turbulent regime as expected:

$$Re_{nf} = \frac{m_{nf}d}{A_t\mu_{nf}} \quad (1)$$

Figure 5 shows variations in Prandtl number, calculated from Eq. (2), with CNT volume concentration. First, Prandtl number decreases for volume fraction of 0.0055% and then increases for higher concentrations. Regarding Prandtl number equation (Eq. 2), the effect of k and c_p is higher than μ for $\phi = 0.0055\%$ because μ is close to the value of water. But increasing ϕ intensifies the effect of μ on Pr resulting in higher Pr value:

$$Pr = \frac{C_p\mu}{k} \quad (2)$$

Figure 6 represents the friction factor evolution versus CNT volume concentration. Friction factor for water and nanofluid flow was calculated with the Gnielinski (Eq. 3) [33] and Duangthongsuk and Wongwises (Eq. 4) [34]

equations, respectively. This figure shows that the friction factor increases with nanotubes concentration.

$$f = [1.58 \ln Re - 3.82]^{-2} \quad (3)$$

$$f = 0.961 Re^{-0.375} \phi^{0.052} \quad (4)$$

Figure 7 shows Nusselt number trend with CNT volume fraction, calculated through Gnielinski relationship [33] and expressed as Eq. 5 for water and various volume concentrations of the CNT–water nanofluid by using previous equations and results:

$$Nu = \frac{(0.125f)(Re - 1000)Pr}{1 + 12.7(0.125f)^{0.5}(Pr^{\frac{2}{3}} - 1)} \quad (5)$$

Increases in Nusselt numbers for 0.0055%, 0.055%, 0.111% and 0.278% volume fractions are about 30%, 32%, 20% and 2.3%, respectively, related to the water. Therefore, increment in the Nusselt number for 0.055% volume fraction is highest related to others.

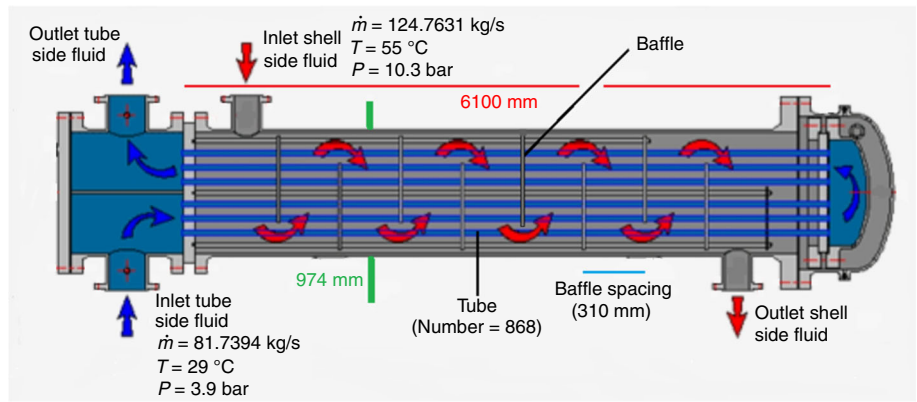
Figure 8 shows the total heat transfer coefficient versus ϕ . According to Eq. 6, Nusselt number and fluid thermal conductivity are proportional to the convection heat transfer coefficient. Increasing the Nusselt number of the fluids to 0.055% CNT volume concentration and increasing thermal conductivity through increasing ϕ result in higher total heat transfer coefficient. Related to others, 0.055% CNT volume concentration possesses maximum total heat transfer coefficient of about 650.7 W m⁻² K⁻¹. For higher concentrations, the total heat transfer coefficient decreases by reducing Nusselt number (Eq. 7).

Heat transfer rate is proportional to total heat transfer coefficient (Eq. 8). Figure 9 shows heat transfer versus CNT concentrations. A maximum heat transfer of about 4133 kW occurs at $\phi = 0.055$ vol% since the total heat transfer coefficient is maximum at this point. The total heat

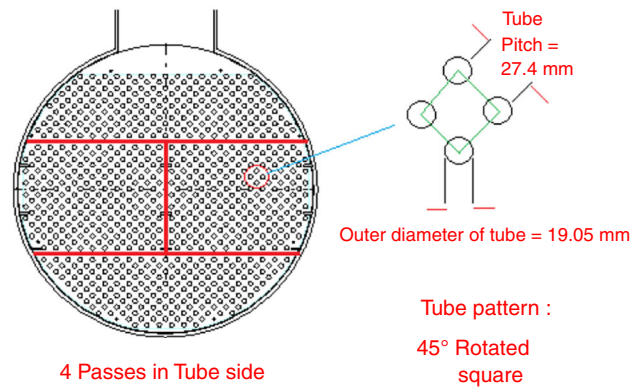
Table 2 Specification of the heat exchanger as well as operational condition of the fluids in shell side (gasoline) and tube side (the coolants)

Parameter	Amount/type	Parameter	Amount/type
Shell inner diameter/mm	950	Baffle type	Single segmental
Shell outer diameter/mm	974	Baffle spacing (center-center) (mm)	310
Tube number	868	Baffle cut %	27
Tube passes per shell	4	Mass flow rate of fluid in shell side (gasoline) (kg s ⁻¹)	124.7631
Tube length/mm	6100	Mass flow rate of tube-side fluid (cooling water and the nanofluid) (kg s ⁻¹)	81.7394
Outer diameter of tube/mm	19.05	Shell-side fluid inlet temperature (°C)	55
Thickness of tube/mm	1.65	Tube-side fluid inlet temperature (°C)	29
Tube pitch/mm	27.4	Shell-side fluid inlet pressure (bar)	10.3
Tube pattern	45-Rotated sqr.	Tube-side fluid inlet pressure (bar)	3.9

Fig. 3 a Schematic figure of the heat exchanger [29]. b. Tube sheet and tube pattern of the heat exchanger schematically



(a)



(b)

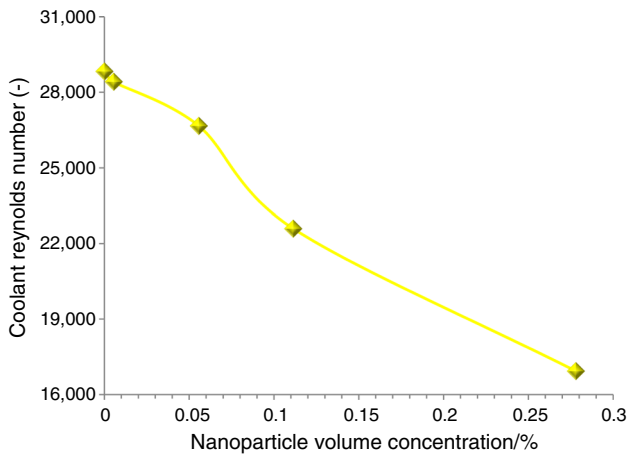


Fig. 4 Re of coolant as a function of CNT loading

transfer coefficient and heat transfer rate for all the CNT concentrations are higher than for water:

$$h_{nf} = \frac{Nu_{nf} \cdot K_{nf}}{d_i} \quad (6)$$

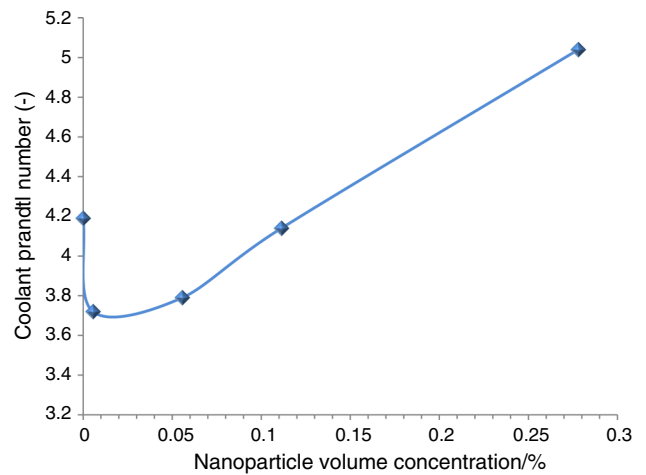


Fig. 5 Coolant Prandtl number as a function of CNT loading

$$\frac{1}{U} = \frac{1}{h_{hot}} + \frac{d_o \ln\left(\frac{d_o}{d_i}\right)}{2k_w} + \frac{1}{h_{nf}} \frac{d_o}{d_i} \quad (7)$$

$$q = UA_s \Delta T_{LMTD} \quad (8)$$

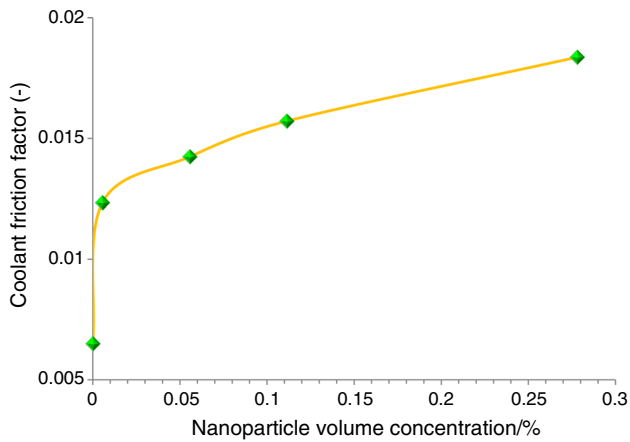


Fig. 6 Coolant friction factor as a function of CNT loading

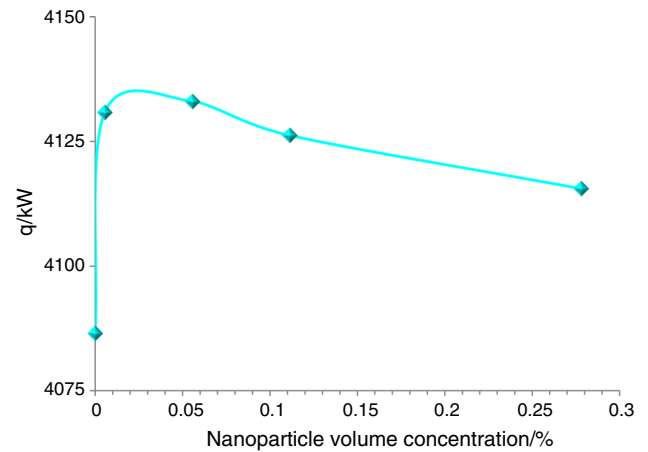


Fig. 9 Heat transfer rate as a function of CNT loading

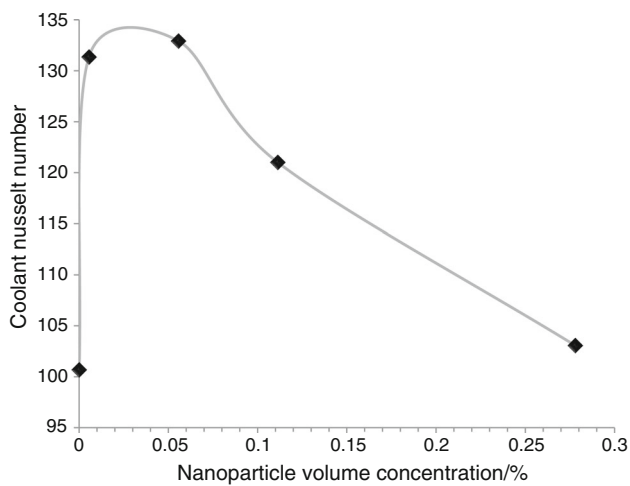


Fig. 7 Coolant Nusselt number as a function of CNT loading

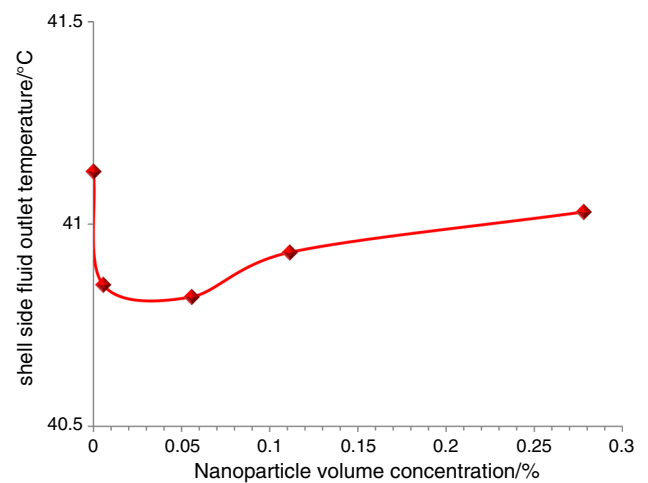


Fig. 10 Outlet temperature of shell-side fluid versus CNT loading

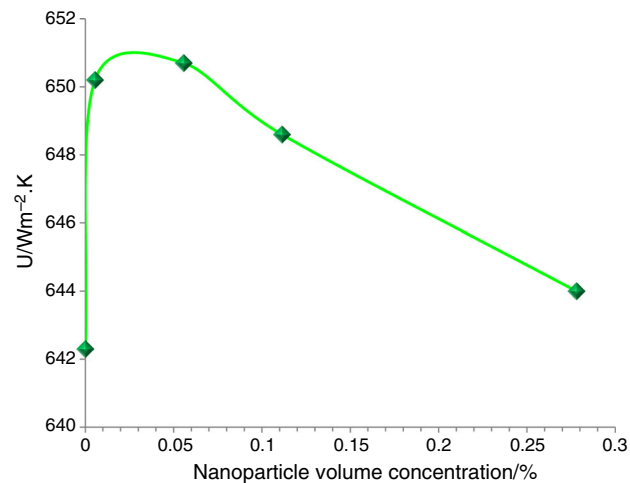


Fig. 8 Total heat transfer coefficient as a function of CNT loading

Since maximum heat transfer rate is obtained for 0.055 vol% CNT nanofluids, the minimum temperature of shell-side fluid outlet occurs at $\phi = 0.055$ as shown in Fig. 10.

Figure 11 illustrates that pressure drop in tube side, provided by the software, increases with CNT concentration, which is directly linked to the increase in viscosity with higher ϕ , and the effect is more prominent at higher ϕ values which have higher pressure loss as well.

Influence of CNT nanofluid mass flow rate on thermal performance

According to Eq. (1), the coolant Reynolds's number is a function of the mass flow rate at a constant ϕ . Hence, when the nanofluid mass flow rate is increased, its Reynolds's number rises too. This explanation is portrayed in Fig. 12. With increment in coolant mass flow rate, Prandtl number also increases for a constant ϕ (Fig. 13).

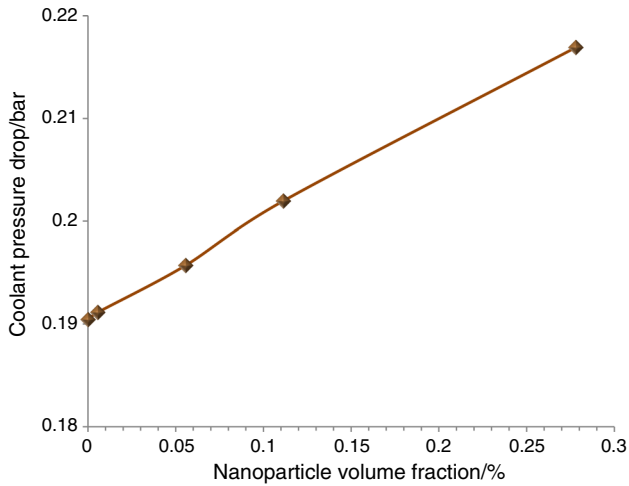


Fig. 11 Coolant pressure drop as a function of CNT loading

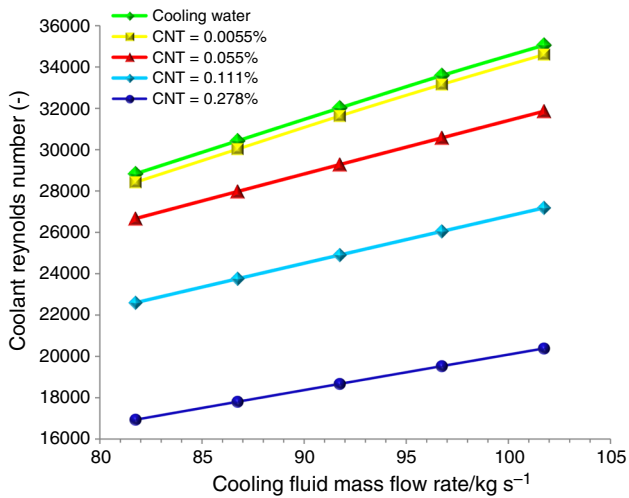


Fig. 12 Effect of m_{nf} on Reynolds number

It would be understood from Eq. 4 that friction factor has an inverse relation with Reynolds number as friction factor decreases with increase in Reynolds number due to the mass flow rate. This trend is demonstrated in Fig. 14. Figure 15 shows that the variations of the items mentioned above due to rise in the coolant mass flow rate result in the increase in Nusselt number. In other words, the rise in coolant mass flow rate causes increment in the Nusselt number for a constant CNT concentration. As can be seen, $\phi = 0.055\%$ possesses the highest Nusselt number.

It is clear from Fig. 16 that as the coolant mass flow rate increases, tube-side pressure drop increases too and also it increases with ϕ . Regarding Eqs. (6–8), the Nusselt number increase makes the total heat transfer coefficient increase (Fig. 17) for all the concentrations. With increase

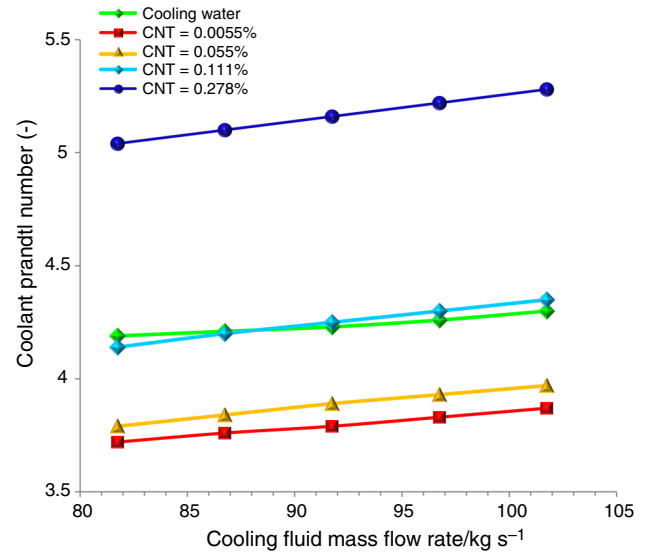


Fig. 13 Effect of m_{nf} on Prandtl number

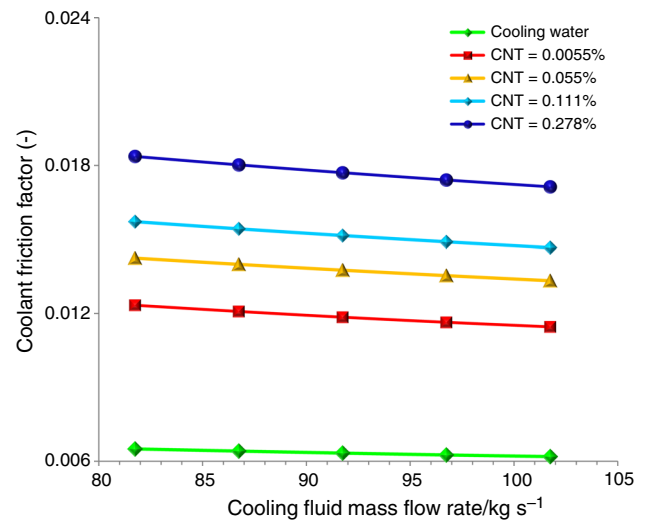


Fig. 14 Effect of m_{nf} on the friction factor

in the total heat transfer coefficient, finally, rise in heat transfer rate happens (Fig. 18), in particular, for $\phi = 0.055\%$, since this loading amount has the maximum total heat transfer coefficient and Nusselt number.

With regards of the heat transfer from the shell side fluid to the tube side cold one, because of the increase of the heat transfer due to mass flow rate, the outlet temperature of the shell side fluid decreases as it is evidenced in Fig. 19. Reasonably, minimum outlet temperature belongs to 0.055% CNT loading since the heat exchanger has highest heat transfer rate with this cooling nanofluid.

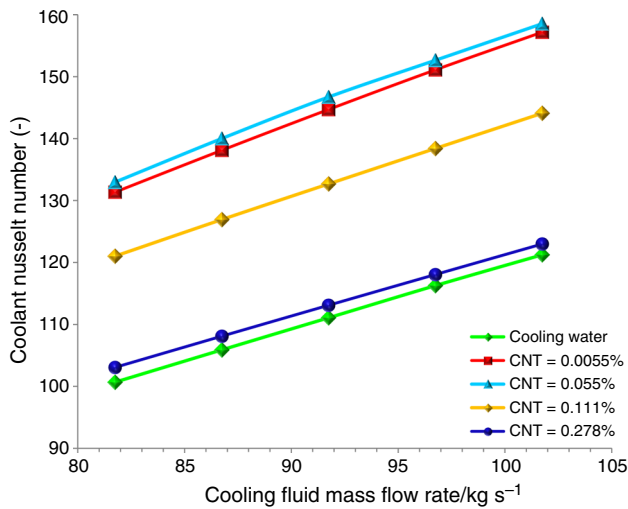


Fig. 15 Effect of m_{nf} on the Nusselt number

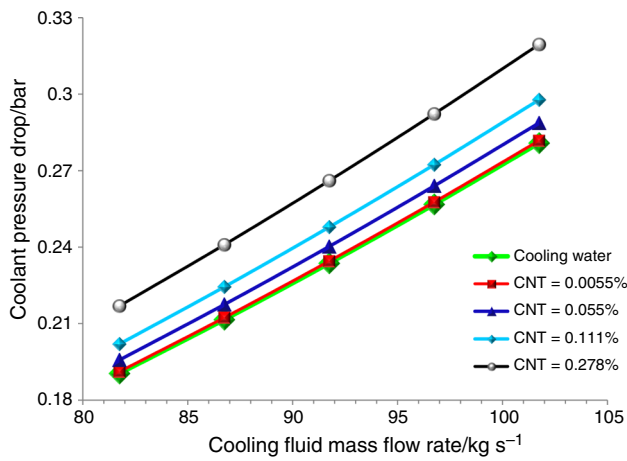


Fig. 16 Coolant pressure drop as a function of m_{nf}

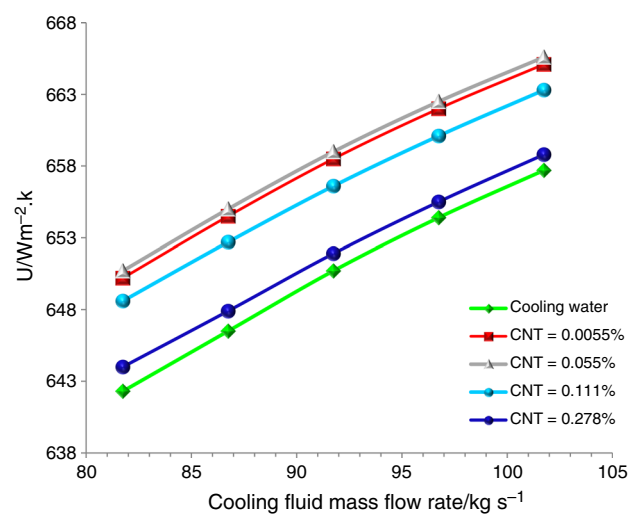


Fig. 17 Effect of m_{nf} on total heat transfer coefficient

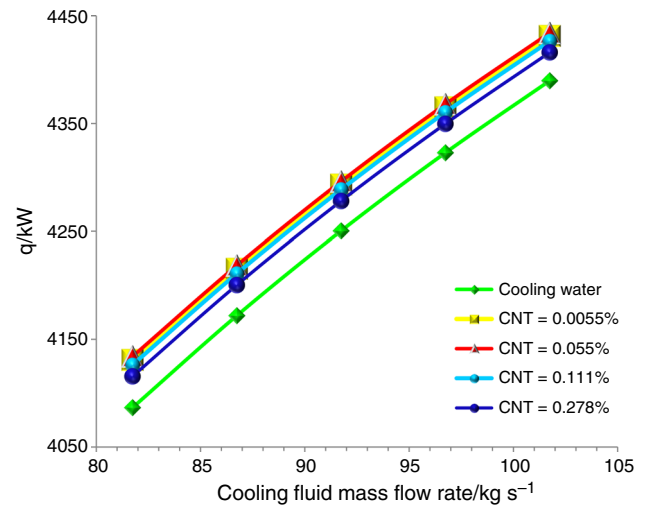


Fig. 18 Effect of m_{nf} on heat transfer rate

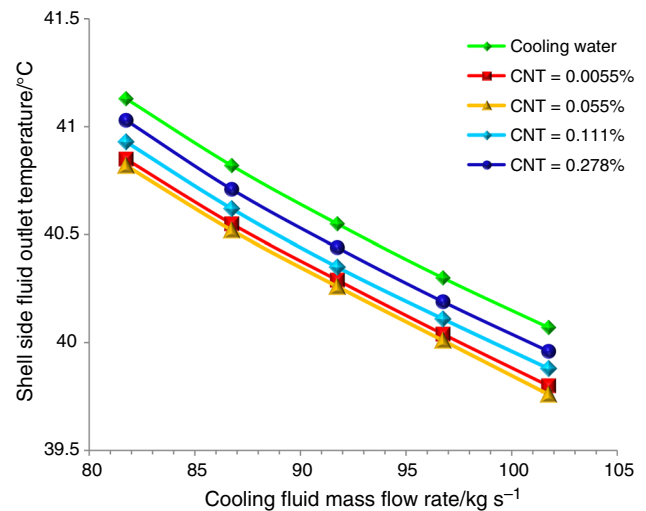


Fig. 19 Shell-side fluid outlet temperature versus the m_{nf}

Effect of shell-side fluid (the gasoline) mass flow rate on thermal performance using CNT-water nanofluid as coolant

Figure 20 shows that the Re of the shell side increases by increasing the mass flow rate \dot{m} based on Eq. (9):

$$Re_{ss} = \left(\frac{m_{ss}}{A_{cf}} \right) \frac{D_e}{\mu_{ss}} \quad (9)$$

Equation (10) [24] shows that higher Re results in higher convection heat transfer coefficient and consequently higher heat transfer rate (Eqs. 7 and 8). As shown in Figs. 21 and 22, increase in shell-side mass flow rate results in higher total heat transfer coefficient and heat transfer rate. Nanofluid coolant results in better thermal performance compared to pure water coolant:

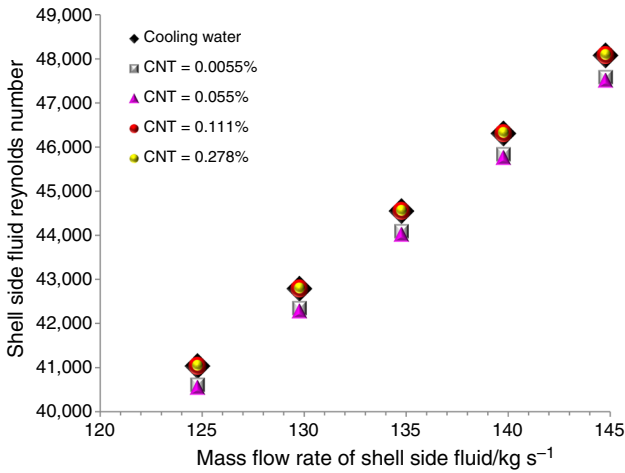


Fig. 20 Reynolds number of shell-side fluid as a function of m_{ss}

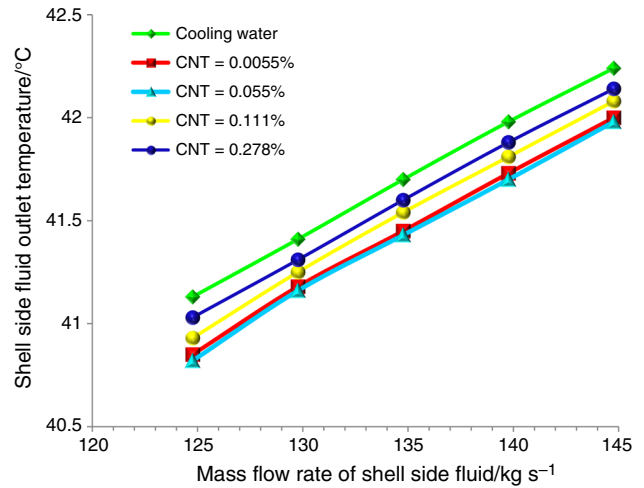


Fig. 23 Effect of m_{ss} on its outlet temperature

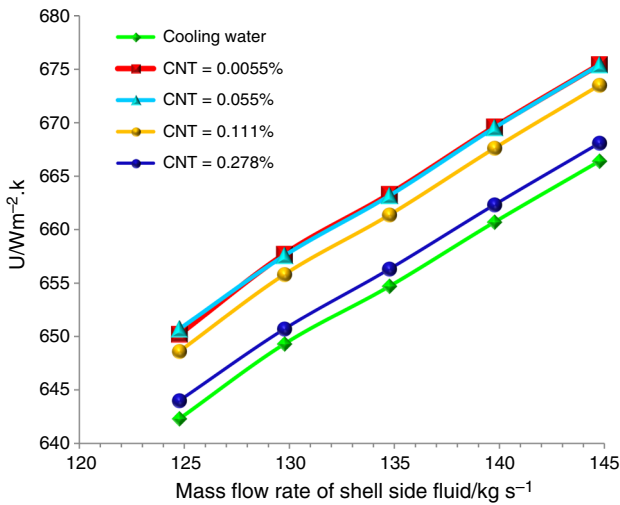


Fig. 21 Total heat transfer coefficient versus m_{ss}

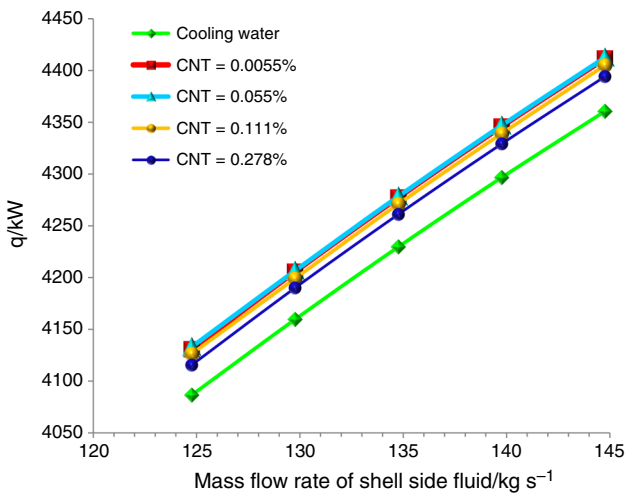


Fig. 22 Heat transfer rate versus m_{ss}

$$h_{ss} = \frac{0.36k}{D_e} Re_{ss}^{0.55} Pr_{ss}^{\frac{1}{3}} \tag{10}$$

Figure 23 represents that with increasing mass flow rate of the hot fluid in shell side, outlet temperature of the shell side would also be increased. But, by comparing the nanofluid as coolant with cooling water, clearly, it can be observed that with a constant mass flow rate of shell-side fluid, the hot fluid outlet temperature is clearly lower when nanofluid is utilized as coolant.

In other words, by using the nanofluid, shell-side hot fluid is less heated related to using cooling water. Thus, by utilizing the nanofluid, viscosity of the shell-side fluid would be higher than cooling water. Therefore, by using the nanofluid, Reynolds number of the shell-side fluid decreases as expressed by Eq. 9. For instance, in Fig. 20, the shell-side fluid Reynolds reduces when water is replaced by nanofluids, especially at $\phi = 0.0055$ and 0.055% . As demonstrated by Fig. 23, the magnitude of the outlet temperature increase for $\phi = 0.055$ is lower than for other concentrations since it causes most heat transfer rate.

Conclusions

This research studied the heat performance of an industrial-scale shell and tube heat exchanger through software simulation by using CNT–water nanofluids as cooling fluids. Results illustrated that all analyzed CNT concentrations improved the heat properties such as Nusselt number, total heat transfer coefficient and heat transfer rate and consequently they enhanced the heat performance of the heat exchanger. This enhancement was also effective to decrease outlet temperature of the shell-side hot

fluid for all CNT volume concentrations. Likewise, there was an optimum CNT concentration corresponding to 0.055 vol% of nanoparticles for which the heat properties reached maximum value and thermal performance of the heat exchanger is optimized. The heat performance enhancement was reached also by increasing mass flow rates of both the cooling nanofluid in all concentrations and the hot fluid in comparison with cooling water. It is also mentioned that optimum concentration of 0.055% also kept the best influence on thermal performance of the heat exchanger with increasing mass flow rates of the fluids in both sides.

References

- Ozsoy A, Corumlu V. Thermal performance of a thermosyphon heat pipe evacuated tube solar collector using silver-water nanofluid for commercial applications. *Renew Energy*. 2018;122:26–34.
- Nakhchi ME, Esfahani JA. Cu-water nanofluid flow and heat transfer in a heat exchanger tube equipped with cross-cut twisted tape. *Powder Technol*. 2018;339:985–94.
- Budak Ziyadanogullari N, Yucel HL, Yildiz C. Thermal performance enhancement of flat-plate solar collectors by means of three different nanofluids. *Therm Sci Eng Prog*. 2018;8:55–65.
- Kim S, Tserengombo B, Noh J, Choi SH, Huh S, Choi B, Chung H, Kim J, Jeong H. Experimental investigation of heat transfer coefficient with Al_2O_3 nanofluid in small diameter tubes. *Appl Therm Eng*. 2019;146:346–55.
- Sidik NAC, Yazid MNAWM, Samion S. A review on the use of carbon nanotubes nanofluid for energy harvesting system. *Int J Heat Mass Transf*. 2017;111:782–94.
- Yanwei H, Li H, He Y, Liu Z, Zhao Y. Effect of nanoparticle size and concentration on boiling performance of SiO_2 nanofluid. *Int J Heat Mass Transf*. 2017;107:820–8.
- Sarviya RM, Fuskele V. Review on thermal conductivity of nanofluids. *Mater Today Proc*. 2017;4:4022–31.
- Bahiraei M, Rahmani R, Yaghoobi A, Khodabandeh E, Mashayekhi R, Amani M. Recent research contributions concerning use of nanofluids in heat exchangers: a critical review. *Appl Therm Eng*. 2018;133(25):137–59.
- Kumar V, Tiwari AK, Ghosh SK. Application of nanofluids in plate heat exchanger: a review. *Energy Convers Manag*. 2015;105:1017–36.
- Mikkola V, Puupponen S, Saari K, Ala-Nissila T, Seppälä A. Thermal properties and convective heat transfer of phase changing paraffin nanofluids. *Int J Therm Sci*. 2017;117:163–71.
- Sani E, Papi N, Mercatelli L, Żyła G. Graphite/diamond ethylene glycol-nanofluids for solar energy applications. *Renew Energy*. 2018;126:692–8.
- Rashidi S, Kashefi MH, Kim KC, Samimi-Abianeh O. Potentials of porous materials for energy management in heat exchangers—a comprehensive review. *Appl Energy*. 2019;243:206–32.
- Shamsabadi H, Rashidi S, Esfahani JA. Entropy generation analysis for nanofluid flow inside a duct equipped with porous baffles. *Therm Anal Calorim*. 2018. <https://doi.org/10.1007/s10973-018-7350-4>.
- Rashidi S, Javadi P, Esfahani JA. Second law of thermodynamics analysis for nanofluid turbulent flow inside a solar heater with the ribbed absorber plate. *Therm Anal Calorim*. 2018. <https://doi.org/10.1007/s10973-018-7164-4>.
- Rashidi S, Akbarzadeh M, Karimi N, Masoodi R. Combined effects of nanofluid and transverse twisted-baffles on the flow structures, heat transfer and irreversibilities inside a square duct—A numerical study. *Appl Therm Eng*. 2018;130:135–48.
- Parizad Laein R, Rashidi S, Abolfazli Esfahani J. Experimental investigation of nanofluid free convection over the vertical and horizontal flat plates with uniform heat flux by PIV. *Adv Powder Technol*. 2016;27:312–22.
- Maskaniyan M, Rashidi S, Esfahani JA. A two-way couple of Eulerian-Lagrangian model for particle transport with different sizes in an obstructed channel. *Powder Technol*. 2017;312:260–9.
- Rashidi S, Mahian O, Languri EM. Applications of nanofluids in condensing and evaporating systems a review. *Therm Anal Calorim*. 2017. <https://doi.org/10.1007/s10973-017-6773-7>.
- Rashidi S, Eskandarian M, Mahian O, Poncet S. Combination of nanofluid and inserts for heat transfer enhancement. *Therm Anal Calorim*. 2018. <https://doi.org/10.1007/s10973-018-7070-9>.
- Mahian O, Kolsi L, Amani M, Estellé P, Ahmadi G, ClementKleinstreuer JS, Marshall RA, Taylor HN, Wongwises S, Hayat T, Kolanjiyil A, Kasaeian A, Pop I. Recent advances in modeling and simulation of nanofluid flows-Part I: fundamentals and theory. *Phys Rep*. 2019;790:1–48.
- Rashidi S, Hormozi F, Sundenc B, Mahian O. Energy saving in thermal energy systems using dimpled surface technology—a review on mechanisms and applications. *Appl Energy*. 2019;250:1491–547.
- Barzegariana R, Aloueyanb A, Yousefic T. Thermal performance augmentation using water based Al_2O_3 -gamma nanofluid in a horizontal shell and tube heat exchanger under forced circulation. *Int Commun Heat Mass Transf*. 2017;86:52–9.
- Shahrul IM, Mahbulul IM, Saidur R, Sabri MFM. Experimental investigation on Al_2O_3 -W, SiO_2 -W and ZnO-W nanofluids and their application in a shell and tube heat exchanger. *Int J Heat Mass Transf*. 2016;97:547–58.
- Hosseini SM, Vafajoo L, Salman BH. Performance of CNT-water nanofluid as coolant fluid in shell and tube intercooler of a LPG absorber tower. *Int J Heat Mass Transf*. 2016;102:45–53.
- Al-Abdali G, Maghrabie HM, Attalla M. Investigation of heat transfer and friction factor of Al_2O_3 nanofluid inside shell and tube heat exchanger. *Sci Eng Res*. 2018;5:549–56.
- Aghabozorg MH, Rashidi A, Mohammadi S. Experimental investigation of heat transfer enhancement of Fe_2O_3 -CNT/water magnetic nanofluids under laminar, transient and turbulent flow inside a horizontal shell and tube heat exchanger. *Exp Thermal Fluid Sci*. 2016;72:82–189.
- Mahian O, Kolsi L, Amani M, Estellé P, ClementKleinstreuer G, Marshall JS, Taylor RA, Niazmand H, Wongwises S, Hayat T, Kolanjiyil A, Kasaeian A, Pop I. Recent advances in modeling and simulation of nanofluid flows-Part II: applications. *Phys Rep*. 2019;791:1–59.
- Estellé P, Mahian O, Maré T, Öztöp HF. Natural convection of CNT water based nanofluids in a differentially heated square cavity. *J Therm Anal Calorim*. 2017;128(3):1765–70.
- Minea AA, Estellé P. Numerical study on CNT nanofluids behavior in laminar pipe flow. *J Mol Liq*. 2018;271:281–9.
- Mohd-Ghazali N, Estellé P, Halelfadl S, Maré T, Choon Sionga T, Abidin U. Thermal and hydrodynamic performance of a microchannel heat sink with carbon nanotubes nanofluids: effect of concentration and channel section. *J Therm Anal Calorim*. 2019. <https://doi.org/10.1007/s10973-019-08260-2>.
- Halelfadl S, Mare T, Estellé P. Efficiency of carbon nanotubes water based nanofluids as coolants. *Exp Thermal Fluid Sci*. 2014;53:104–10.

32. www.korenergy.co.kr.
33. Gnielinski V. New equations for heat and mass transfer in turbulent pipe and channel flow. *Int Chem Eng.* 1976;16:359–68.
34. Duangthongsuk W, Wongwises S. Heat transfer enhancement and pressure drop characteristics of TiO₂–water nanofluid in a double-tube counter flow heat exchanger. *Int J Heat Mass Transf.* 2009;52:2059–67.

Publisher's Note Springer Nature remains neutral with regard to jurisdictional claims in published maps and institutional affiliations.